Editorial Manager(tm) for Monthly Weather Review
Manuscript Draft

Manuscript Number: MWR-D-11-00005

Title: Isentropic Descent Beneath the Saharan Air Layer and its impact on Tropical Cyclogensis

Article Type: Article

Corresponding Author: Michael Diaz

Corresponding Author's Institution: North Carolina State University

First Author: Michael Diaz

Order of Authors: Michael Diaz;Anantha Aiyyer;Fredrick Semazzi

Abstract: We investigate the driving mechanism behind strong climatological isentropic descent in the eastern Atlantic and how it affects tropical cyclogenesis from African Easterly Waves (AEW). Our results suggest that this isentropic descent is forced by the warm thermal structure associated with the Saharan Air Layer (SAL) combined with northerly flow on the eastern flank of the Azores high. Since this northerly flow descends from the drier middle troposphere at higher latitudes to the lower troposphere at lower latitudes, it provides a nearly continuous source of dry air off the West African coast. Thus, AEWs traveling south of the SAL often ingest dry air from the middle latitudes into their circulation. Once ingested by an AEW, this dry air mass may suppress the moist convection required for tropical cyclogenesis. Although this process is intimately linked with the SAL, the air mass involved is distinctly different; it originates from the middle latitudes and travels beneath the SAL. In contrast, previous studies emphasize the direct negative impacts of the SAL itself on tropical cyclogenesis and concentrate primarily on how strong vertical wind shear, dry mid-level air, and high static stability suppress AEW convection.

Suggested Reviewers:

Opposed Reviewers:

Isentropic Descent Beneath the Saharan Air Layer and its impact on Tropical Cyclogensis

Michael Diaz *

Department of Marine, Earth, and Atmospheric Sciences, Raleigh, NC

Anantha Aiyyer

Fred Semazzi

Department of Marine, Earth, and Atmospheric Sciences, Raleigh, NC, USA

* *Corresponding author address:* Michael Diaz, NCSU Raleigh, NC 27695.

E-mail: mldiaz@ncsu.edu

ABSTRACT

We investigate the driving mechanism behind strong climatological isentropic descent in the eastern Atlantic and how it affects tropical cyclogenesis from African Easterly Waves (AEW). Our results suggest that this isentropic descent is forced by the warm thermal structure associated with the Saharan Air Layer (SAL) combined with northerly flow on the eastern flank of the Azores high. Since this northerly flow descends from the drier middle troposphere at higher latitudes to the lower troposphere at lower latitudes, it provides a nearly continuous source of dry air off the West African coast. Thus, AEWs traveling south of the SAL often ingest dry air from the middle latitudes into their circulation. Once ingested by an AEW, this dry air mass may suppress the moist convection required for tropical cyclogenesis. Although this process is intimately linked with the SAL, the air mass involved is distinctly different; it originates from the middle latitudes and travels beneath the SAL. In contrast, previous studies emphasize the direct negative impacts of the SAL itself on tropical cyclogenesis and concentrate primarily on how strong vertical wind shear, dry mid-level air, and high static stability suppress AEW convection.

1. Introduction

African Easterly Waves (AEWs) are the most common precursors to tropical cyclones over the Atlantic (e.g. Carlson and Prospero (1969), Carlson (1969), and Thorncroft and Hodges (2001)). However, as noted by these studies, very few AEWs actually generate tropical cyclones. For example, using a dataset from 1967-1995, Pasch et al. (1998) identify an annual average of 61 AEWs, but only nine Atlantic tropical storms. However, 62% of

these tropical storms originate from AEWs. The rarity at which AEWs generate tropical cyclones is primarily a consequence of the limiting effect of environmental factors such as ocean heat content, vertical shear and low level moisture (e.g. Gray (1968)). More recently, there has been increased interest in the effects of the Saharan Air Layer (SAL) on AEWs and tropical cyclogenesis. Carlson and Prospero (1972) conducted one of the pioneering studies on the SAL. They found that the SAL originates from the intense radiative heating over the Sahara. This heating generates a deep mixed boundary layer, which is advected by the African easterly jet (AEJ) into the eastern Atlantic, where it rises above the trade wind inversion and forms a nearly adiabatic layer between 850 hPa and 500 hPa. The SAL is characterized by high potential temperature, high dust concentrations, and low relative humidity. Consistent with a minimum in mid-level moisture during June and July over the eastern Atlantic (DeMaria et al. (2001)), it peaks in intensity during early summer.

It remains unclear whether the SAL has a positive or negative influence on AEWs and tropical cyclogenesis. Karyampudi and Carlson (1988) and Karyampudi and Pierce (2002) suggested that the SAL helps to maintain or amplify some AEWs in their early stage of development by imposing strong baroclinicity east of the wave axis and promoting transverse vertical motions. However, they also noted that heavy dust, especially during June and July, tends to suppress cumulus convection and thus may be particularly detrimental to AEWs in early summer. Karyampudi and Pierce (2002) extended this work by examining three tropical cyclones in relationship to the SAL. They concluded that the SAL had a positive influence on two cases, which occurred during wet Sahel years, and a negative influence on one case, which occurred during an extremely dry Sahel year. However, one could argue that the limited sample size of this study and the competing factors influencing tropical

cyclogenesis seem to complicate the interpretation of these results.

Dunion and Velden (2004) found that the SAL suppresses tropical cyclone activity by introducing dry, stable air into incipient tropical cyclone circulations, increasing vertical wind shear, and enhancing the pre-existing trade wind inversion. In contrast, Braun (2010) downplays the role of the SAL in affecting tropical cyclones. He notes that dry air is not a defining characteristic of the SAL since it is already located in a region of large scale descent, and that much of the dry air in the eastern Atlantic is of non-SAL origin. He suggests that previous work on tropical storm Debby (2006) incorrectly attributes its demise to dry air associated with the SAL, since that dry air was free of dust. Braun (2010) proposes that one should not simply blame the SAL for the weakening of a tropical cyclone just because it is nearby, but rather clearly demonstrate that it had a negative impact.

Extending earlier work on the SAL's influence on AEWs, the focus of this study is another potentially important consequence of the SAL which has thus far received little treatment; it induces strong climatological isentropic descent along the African coast north of AEWs. The objective of this study is to describe this process and how it may impact AEWs and subsequent tropical cyclogenesis.

The presence of strong isentropic descent in both subtropical deserts and the eastern flank of subtropical highs is discussed at length in Rodwell and Hoskins (1996) and Rodwell and Hoskins (2001). In these two studies, subtropical deserts are attributed to the intense latent heat release in the wet summer monsoon regions, which instigates isentropic descent to the west. Whereas those studies stress the importance of monsoons in forcing isentropic descent to the west, we emphasize the role of the SAL and the Azores High in localizing isentropic descent near the surface along the African coast.

Analogous to the latent heat release in the Asian monsoon, the intense radiative heating in the Sahara, which generates the SAL, acts to depress the isentropes toward the surface over the eastern Atlantic. Thus, the mid-latitude westerlies interacting with the northern edge of the SAL undergo isentropic descent beneath the base of the SAL as they turn southward around the Azores High. The northerly winds on the eastern flank of the Azores High convey this mid-latitude air southward, where it may interact with AEWs traveling south of the SAL. In fact, since the anomalous circulation of an AEW may extend north of 30°N along the northwest African coast (Kiladis et al. 2006), AEWs themselves may assist in this process. However, it is important to point out that most equatorward flow descends isentropically due to the mean equatorward directed temperature gradient. The process illustrated here is merely a localized accentuation of this descent.

Unlike other recent studies which emphasize the negative influence of the dry air within the SAL on convection, our results suggest that much of the dry air within AEWs at lower levels is actually of mid-latitude origin; isentropic descent beneath the SAL brings this dry, mid-latitude air from aloft to lower levels. The idea of isentropic descent beneath the SAL fits loosely into the conceptual model of the SAL presented by several earlier studies. Carlson and Prospero (1972) mention "the low-level coastal flow of dust-free air from the northern latitudes" and show this feature in their Fig. 20. Karyampudi and Carlson (1988) state that "the base of the SAL is always elevated, due to the undercutting of cool trade wind air beneath the desert mixing layer," and they show this process in their Fig. 1. Our results show that these "undercutting" trade winds along the African coast extend into the region of strong isentropic descent to the north and provide a nearly continuous source of dry air from aloft in the mid-latitudes to near the surface in the tropics. It is also consistent with

the results of Braun (2010), which finds that there are other sources of dry air in the eastern Atlantic beyond the SAL.

2. Methodology

The primary goal of this work is to demonstrate how the SAL forces isentropic descent in the eastern Atlantic and to investigate how this process influences AEWs. Using a large sample of AEWs, we estimate how much air within AEW has a history of isentropic descent along the northwest African coast. We then examine which regions of the AEW and which altitudes tend to contain this airmass and determine whether or not it is detrimental to AEW convection and future tropical cyclogenesis. We also investigate the history of this airmass before it reaches AEWs and how it varies seasonally.

a. Dataset

The dataset used in all of our analyses is the 1.0° x 1.0° Global Forecast System (GFS) Final (FNL) analysis. This analysis is available at six hourly intervals on 26 pressure levels from 2000 to 2008. The FNL version uses the GFS operational model, but the data assimilation system is run at three hours past synoptic time to allow more data to be assimilated and to use a shorter forecast lead time.

b. Case Selection

In order to sample a large number of AEWs in the eastern Atlantic which could serve as tropical cyclone precursors, we use an automated vortex identification algorithm. To focus on the eastern Atlantic, we limit the domain to 7°-16°N and 30°-24°W. This algorithm searches for persistent maxima in isentropic relative vorticity averaged over the 302 K - 306 K layer, which corresponds roughly to the 800-900 hPa layer in the tropical eastern Atlantic. The outline of the algorithm is given below.

i. A potential wave is identified as a local maximum in curvature vorticity. The choice of using only the curvature vorticity eliminates the impact of horizontal wind shear and better distinguishes closed circulation centers from the persistent African easterly jet near the southern fringe of the SAL. Berry et al. (2007) also resort to curvature vorticity.

ii. The area-average vorticity within a 300 km radius of each potential AEW must exceed $1.5\text{x}10^{-4}s^{-1}$. Though somewhat arbitrary, this threshold seems to best separate larger AEWs circulations from smaller scale noise.

iii. To ensure temporal and spatial coherency, each AEW must exist for at least three consecutive time periods (i.e. a total of 18 hours) and must be within 4.0° west or 1.0° east of its previous location. Once a case is identified, we choose for subsequent analysis the time and location at which the area average vorticity is at a maximum.

Our tracking algorithm identifies 191 separate AEWs over the course of nine years. This amounts to an average of 21 AEWs per year, a standard deviation of 2.9, a minimum of 16,

and a maximum of 25. Although this average is much smaller than that calculated by Pasch et al. (1998) (61 AEWs), it is close to the results of Hopsch et al. (2007). The seemingly large discrepancy likely results from different AEW identification techniques. The method we use targets only stronger, more coherent systems in a limited region and therefore likely excludes many weaker systems.

To test the impact of the isentropically descending air on tropical cyclogenesis, we separate the identified waves into "developing" and "non-developing" cases. To make this distinction, we use the NHC's preliminary reports to connect each tropical depression or tropical storm with an AEW. Since the process we are studying is limited to the eastern Atlantic, we consider an AEW as developing only if it forms at least a tropical depression east of 60° W. Moving this boundary east or west by 10° has a negligible effect on our conclusions.

c. Trajectories

To support our argument that much of the dry air within AEWs originates from mid-latitudes, we perform six day isentropic trajectory analysis. Back trajectories for air parcels are started every 1 K within a 299-309 K potential temperature vertical layer and every 0.5° within a 5° x 5° horizontal box centered on each identified AEW. Additional analysis suggests that almost all of the dry air advection from isentropic descent occurs within this layer and that air parcels with temperatures less than 309 K are too cool to have originated recently within the SAL.

Since many of the air parcels undergoing isentropic descent reach very low altitudes (below 900 hPa) and pass directly adjacent to the African coast, they appear to intersect the

surface, since boundary layer potential temperature onshore often exceeds 309 K. Assuming these parcels do not in reality intersect the surface and are too cold to originate from the Sahara, we attribute this problem primarily to the coarse temporal and spatial resolution of the 1.0°x1.0° GFS, which does not resolve the strong temperature gradient near the African coast well enough to track parcels near that coast. Any small errors in the trajectory calculation or a misrepresentation of this temperature gradient can send parcels which should remain over the ocean crashing into the coastline. Since the region near Cap Blanc (18°-21°N), where the land juts out into the ocean, seems to be the farthest south that southward moving air parcels frequently intersect the ground, we define a box whose southern boundary is 18°N and whose western boundary extends along a line from 18°N, 25°W to 33°N, 15°W. This box roughly confines the region of enhanced dryness resulting from isentropic descent (see Fig. 2). The eastern boundary naturally occurs where the isentropes intersect the surface near the coast, beyond which most parcels are calculated to intersect the ground. Moving the western boundary of this box west has little effect on the number of trajectories passing through this region, while moving it east slowly cuts off the more westerly trajectories. Despite obvious deficiencies with this methodology, the results indicate that it is successful in identifying low level dry air intrusions in AEWs. As such, the correct terminology for this airmass is "low level air from mid-latitudes with a history of significant isentropic descent along the African coast." For simplicity, we will refer to it as "isentropic descent".

To better understand the typical history of isentropic descent, trajectories locations and characteristics are composited by binning each point along the trajectory according to latitude and averaging. Constraining the trajectories to a narrow region along the African coast forces them to follow a similar path and thus justifies this averaging technique.

d. Composite Fields of AEWs

To determine how isentropic descent affects the structure of AEWs, we create wave-centered composites of various fields. This is done by shifting data grids such that the vorticity maximum for each wave lies at a reference location. Composite categories are defined depending on the fraction of isentropic descent ingested into wave circulation and whether or not tropical cyclogenesis ensues.

e. Statistical Significance Testing

We test whether the differences between developing and non-developing systems is statistically significant by calculating p-values. Since many of our distributions are highly skewed, we use Monte Carlo simulations to determine p-values. They are calculated by randomly selecting samples from the entire population to generate two new subsets. The average difference between these two new subsets is calculated and compared to the difference between the original subsets (e.g. developing and non-developing systems). This procedure is iterated 100,000 times. The p-value is the number of times the mean difference between randomly generated subset exceeds the difference between the two original subsets divided by the number of iterations.

3. Results

a. Climatology of Isentropic descent

To illustrate the process of isentropic descent, we present the mean July to September (JAS) pressure, winds, and mixing ratio on the 303 K isentropic surface (Fig. 1). Offshore, and along the African coast, there is a steep isentropic pressure gradient, which is a manifestation of the strong temperature gradient between the hot Sahara and the much cooler marine air mass. Consistent with this strong gradient, the 303 K isentrope dips sharply toward the surface near the African coast. The SAL is clearly evident between 10°N and 25°N in the eastern Atlantic, where the 303 K isentrope dips toward the surface. Since the temperature gradient vector is oriented perpendicular to the African coast, thermal wind balance dictates that the flow become increasing parallel to the coast as air moves southward from aloft to near the surface.

Since the average mid-latitude westerly flow at 303 K is located between about 800 hPa and 750 hPa, and has mixing ratios of less than 6 g/kg, this pattern provides a nearly continuous flow of dry air southward along the African coast, beneath the SAL. As a further illustration of this process, we examine average 925 hPa mixing ratio in the eastern Atlantic (Fig. 2). The most striking feature of this analysis is the elongated area of reduced mixing ratios offshore along the African coast, extending northward to Portugal. With mixing ratio below 6 g/kg in the mean, this area is drier than coastal inland regions. While similar mixing ratios can be seen over interior Sahara, the winds are primarily northerly offshore. Thus the acute dryness does not seem related to the desert. Based on Fig. 1, the source of this dry air seems to be in the mid-latitudes, and it is brought to low levels by isentropic descent beneath

the SAL. The driest air at 925 hPa occurs between 20°N and 27°N, where the isentropes dip closest to the surface.

Fig. 3 shows the average 975- and 600-hPa winds. Above 800 hPa, warmer Saharan air rises above the marine boundary layer inversion and is transported offshore into the Atlantic or northeastward toward Europe. Below 800-hPa, northerly flow in the eastern Atlantic associated with the Azores High undercuts the SAL.

From the preceding analyses, the cause of the isentropic descent in this region becomes clear; mid-latitude westerly winds interacting with the northern fringe of the SAL are forced by the strongly sloping isentropes to turn southward via thermal wind balance. This process constantly conveys dry mid-latitude air from aloft into the tropical eastern Atlantic beneath the SAL.

b. Trajectory Analysis

Figure 2 shows a map of the 301 K composite trajectory overlaid with the average 925-hPa mixing ratio for the JAS months. The average height, wind speed, mixing ratio and time rate of change of mixing ratio following trajectories at several levels between 301 K and 307 K are shown in Fig. 4(c). From Fig. 4(a), isentropic descent is clearly seen as air parcels drop approximately 1 km between 46^o and 24^o. In the northwestern most extent of their trajectories, parcels are embedded within the mid-latitude westerlies as they travel around the northern and eastern flank of the Azores high. Their generally southeastward path carries them toward the coast of Portugal and Africa, where they decelerate, turn sharply southward, and are forced by the warmer SAL to descend. Although the location of

this sharp turn varies greatly from case to case (not shown), once parcels reach as far south as 30°N, they follow a narrow channel along the coast. As noted earlier, this sharp turn is consistent with thermally balanced flow associated with the nearly stationary baroclinic zone at the coast which separates hot Saharan air from cooler, marine air.

Since most of the trajectories still remain above 1 km north of 35°N, little moistening occurs, with mixing ratio increasing by only about 0.25 g/kg per day (Fig. 4(d)). The exact rate of moistening probably depends on how close to the coast an air parcel travels, since parcels traveling near the coast will remain at a lower altitude and are thus exposed to stronger surface moisture fluxes.

As air parcels travel from 35°N and 22°N, they continue to descend beneath the thickening SAL, but at a slower rate than previously. The plot of 925 hPa mixing ratio (Fig. 2) clearly shows the impact of this descent as an elongated region of lower mixing ratios immediately offshore. Continued descent squeezes the isentropes into a thin layer near the surface and leads to extremely high low level static stability (Fig. 4(a)). This process creates an inversion which limits mixing between the SAL and the marine boundary layer; only parcels traveling beneath the SAL are exposed to moisture fluxes from the underlying ocean. Consequently, as they descend to their lowest altitude near 22°N, their rate of moistening rapidly increases to a maximum near 22°N (Fig. 4(d)). This moistening is a function of height, as 301 K parcels moisten at about 2.5 g/kg per day at 22°N and 307 K parcels at about 1.5 g/kg. Despite strong moistening rates, mean wind speeds of 9-11 m/s limit the integrated effect of this moistening and the flow can thus remain relatively dry.

Between 20°-25°N, the descending flow reaches its lowest altitude above the ocean. As seen from Fig. 4(b) , wind speed reaches a maximum and, consistent with thermal wind

balance, forms a low level jet. This local wind maximum is likely due to the Bernoulli effect; where the flow is squeezed into a smaller volume, it must travel faster to maintain mass continuity, assuming it is nearly incompressible. Therefore, the maximum wind speed exactly coincides with the maximum in static stability and minimum in parcel height. This relationship also manifests itself in Fig. 2, where a local wind maximum is collocated with the mixing ratio minimum. Based on the previous description, air offshore northwestern Africa should be driest where descending parcels reach their lowest height. Coincidentally, these strong winds occur at the coast, where they induce upwelling (not shown). Cold SST resulting from upwelling enhances the low level temperature inversion and thus helps to further prevent mixing between the SAL and the marine boundary layer. Thus, there may be a positive feedback process between SST, wind speed, and dry air.

The flow properties change once again as air parcels travel south of 22°N toward AEW circulations. The overlying SAL becomes thinner and air parcels consequently begin a slow ascent (Fig. 4(a)). Since air parcels at higher altitudes rise faster than those at lower altitudes, isentropes spread apart vertically and static stability decreases. By the time this air mass reaches AEWs near 13°N, the 300-305 K air column has approximately tripled in depth from its value near 22°N. This increase in mass between isentropes requires a mass flux convergence, which is provided by a rapid decrease in wind speed (Fig. 4(b)). As parcels move farther offshore south of 22°N (Fig. 2), they leave the baroclinic and wind shear consequently decreases along the trajectories (Fig. 4(b)). Additionally, since the flow is farther aloft and has already undergone substantial moistening, moistening rates decrease (Fig. 4(d)).

c. Quantity of Isentropic Descent within AEWs

1) Horizontal Distribution

The frequency of isentropic descent is calculated at each location within the 301-304 K layer at which a back trajectory begins (i.e. every 0.5° and every 1 K) within a 5° x 5° box centered on each AEW. For each point, we calculate the percent of cases which contain isentropic descent and average this percent over all five levels within the 301-304 K layer. This procedure produces a wave-centered plan view map showing the frequency at which isentropic descent occurs within AEW circulation. For reference, we overlay the wind velocity field averaged over all cases. The results for all AEWs, as well as separated for developing and non-developing waves are shown in Figure 6.

The following observations can be made regarding the spatial distribution of isentropic descent for all AEWs (Fig. 6(a)).

i. About 400 km northwest of the mean AEW circulation, isentropic descent is present for more than 80% of the cases.

ii. Near the circulation center, isentropic descent is present in about 55% of cases

iii. About 400 km southwest of the circulation, isentropic descent is present in fewer than 20% of the cases.

iv. The region of higher frequency within 0-300 km northeast of the circulation center appears to be associated with the cyclonic wrapping of isentropic descent around the back side of the circulation.

v. The small region of lower frequency 0-100 km southeast of the center, which forms a small notch, may be associated with air parcels which loop around the center for extended periods of time and thus do not track far from their initial location relative to the AEW center.

Thus, higher frequencies of isentropic descent occur over the northwestern region and lower frequencies over the southeastern region. This pattern should be expected, since northerly winds ahead of the circulation are more likely to have originated from the north, where isentropic descent originates.

Separating developing from non-developing cases reveals substantial differences (Figs. 6(b), 6(c), 6(d)) and suggests that isentropic descent has a negative impact on tropical cyclogenesis. The key observations are:

i. The largest differences are concentrated in the northeastern quadrant of the circulation, with values between 40% and and 60%.

ii. The fraction of isentropic descent within the rest of the circulation generally differs by less than 15%.

iii. A comparison of Fig. 6(b) and Fig. 6(c) suggests that the northwestern quadrant of AEWs nearly always has isentropic descent, while the southern two quadrants contain isentropic descent much less frequently (Fig. 6(a)).

Thus, the biggest room for differences between developing and non-developing AEWs occurs in the northeastern quadrant. Based on current models of tropical cyclogenesis, one may expect that, if isentropic descent is detrimental to tropical cyclogenesis, it would be

most destructive once it wraps through and around the backside of the center of circulation, where it can suppress the convection near the circulation center. This brings into the picture the potential importance of the scale and strength of the wave itself in determining the extent of ingestion of descending air. This issue needs additional scrutiny.

2) Vertical Distribution

For each AEW, using the trajectory data, we determine the extent of isentropic descent within 300 km of its center at different levels between 299 K and 309 K. We deem the air mass within this small radius to be important since tropical cyclogenesis requires convection to be collocated with the low level circulation center and 600 km is the approximate diameter of a typical tropical cyclone. Altering this value by about 100 km has a negligible effect on our general conclusions. We place each AEW into one of following five categories: 0-20%, 20-40%, 40-60%, 60-80%, and 80-100%. The percentage denotes the fraction of the circulation within 300 km that had a history of isentropic descent for that wave. Figure 8 shows the number of AEW cases (out of a total of 191) falling into these categories as a function of the isentropic level.

This analysis shows that many AEWs contain a significant fraction of isentropic descent at low levels. Although our results suggest a peak at 301 K (which corresponds to about 915 hPa at 13° N), this outcome is likely artificial, since many of the calculated trajectories below this height intersect the ground near the African coast. As evidence of this deficiency, note the spike in cases falling into the 0-20% category at 299 K. Therefore, this methodology likely significantly underestimates the fraction of isentropic descent below 301 K. Above this

level, the fraction of isentropic descent also decreases, and this outcome is consistent with the weakening northerly flow with height along the northwest African coast. Additional analysis (not shown) suggests that above 305 K, an increasing fraction of airmass originates from continental Africa, south of the Sahara. This shift in prevailing flow direction partially explains the large increase in systems falling within the 0-20% category and limits the importance of isentropic descent above 305 K.

3) Quantity of Isentropic Descent and Tropical Cyclogenesis

We hypothesize that entrainment of isentropic descent is detrimental to AEW convection and the probability that an AEW will undergo tropical cyclogenesis since isentropic descent tends to be very dry. As a test, we compare the characteristics of developing and non-developing AEWs. Table 1 shows the mean latitude of the AEWs, and average and median values of the percentage of circulation with isentropic descent within 300 km of the wave center.

The key results are summarized below:

i. The average quantities of isentropic descent within 300 km of wave center are respectively 57% and 73% for developing and non-developing cases. With a p-value of 0.01, this difference seems robust.

ii. Since our distribution is strongly skewed toward higher fractions of isentropic descent, using the median as a comparison yields even larger differences: 85% for non-developing cases and 50% for developing cases. The difference between the two are again statistically significant.

iii. On average, developing cases during July and August have 22% less isentropic descent than non-developing cases with a p-value of 0.18 for July and 0.01 for August. Since July has only five developing cases, not enough data are available for statistically significant results.

iv. Developing cases in September average 2% higher than non-developing cases with a median difference of 1% less. Since the p-value for this mean difference is 0.81, it appears that isentropic descent has little effect on tropical cyclogenesis during September.

As an alternative comparison, we break down the AEW cases by fraction of isentropic descent and organize them into three categories: 0-40%, 40-80%, and 80-100% (Table 2). We decided upon an uneven partition to make the number of cases in each category more uniform. The conclusions from this analysis are similar to those of the previous; cases in July and August which ingest a significant quantity of descending air have a smaller probability of developing compared with those with a smaller faction. For example, during August, 56% of cases in the 0-40% category develop compared to only 17% in the 80-100% category. Similar to the previous analysis, isentropic descent does not appear detrimental to tropical cyclogenesis by September.

These results suggest that isentropic descent negatively impacts tropical cyclogenesis. However, this effect seems less important in September compared to July and August. There are several possible explanations for this. As SST along parcel trajectories into AEWs increases through September, descending air undergoes more significant modification. In fact, average SST near the southern oceanic upwelling region along northwest Africa increases by over 3°C from June to September (not shown). To test this idea, we break down the along

trajectory mixing ratio (Fig. 4(c)) by month (Fig. 5). North of about 30°N, mixing ratio does not vary much among JAS. However, once it reaches latitudes typically traversed by AEWs, there is a 3-4 g/kg increase in mixing ratio from July to September. This seasonal change likely makes isentropic descent less detrimental to AEW convection later in the summer.

Additionally, DeMaria et al. (2001) point to the increasingly detrimental impact of strong vertical wind shear toward September in the eastern Atlantic. Though atmospheric stability properties are most favorable for tropical cyclones in September, their results suggest that increasing wind shear causes tropical cyclone frequency to decrease after about the first week of September. Additionally, AEWs in September follow a more southerly latitude (10.6°N against 12.5°N for August; Table 1). A southward shift in track for September AEWs is consistent with the results of Hopsch et al. (2006). We speculate that the impact of isentropic descent is less severe in September since the waves are farther removed and the descending air has more time to be modified. This intraseasonal difference in the effect of isentropic descent requires further scrutiny.

d. AEW Structure

1) Impact of Isentropic Descent on AEWs

To investigate how isentropic descent impacts AEWs, we compare composites of selected meteorological fields for our cases organized by the fraction of isentropic descent contained within a 300 km radius of the circulation center. As in the analysis shown in Table 2, we partition all waves into three categories, 0-40%, 40-80%, and 80-100%, where the percent denotes the fraction of the wave circulation within 300 km having a history of isentropic

descent. Figure 9 shows the composite 303 K mixing ratio and winds, 500 mb vertical velocity, and the 301-305 K lapse rate. As demonstrated before, the 303 K level lies beneath the SAL. The 500 mb vertical velocity serves as a proxy for convection.

The 80-100% composite AEW (Fig. 9(c)) is nearly devoid of convection within 200 km of its circulation center, but contains a broad band of convection well to its south. Considering that the center of our cases averages near 12°N, this convection would typically be centered near 6°N, which places it within the intertropical convergence zone (ITCZ). The dry air associated with isentropic descent is clearly apparent in the northwest quadrant. Near the center, isentropic descent and moister air from the south are wrapping around each other cyclonically.

In the 40-80% composite (Fig. 9(b)), there is a definite northward shift in the convection and it now lies directly over the circulation center. However, it still has a southward bias as the dry air from isentropic descent seems to be eroding the northern edge of the convection ahead of the circulation. Nevertheless, in comparison with the 80-100% composites, this composite seems much more likely to become a tropical cyclone since the convection is collocated with the circulation center. Recall from Table 2 that 16% of cases in the 80-100% category undergo tropical cyclogenesis compared to 26% of cases in the 40-80% category.

The 0-40% composite (Fig. 9(a)) follows a similar trend; convection shifts northward and appears stronger with lower fraction of dry air in the northwestern quadrant. Of all the cases in this category, 37% eventually become tropical cyclones (Tab. 2). Surprising, Fig. 9(a)) and Fig. 9(b) also reveal that precipitation is strongly favored ahead of these AEWs, where the air tends to have a history of isentropic descent. Though seemingly contradictory, further analysis (not shown) demonstrates that, since these AEWs circulations are in a region

where the temperature gradient points northward, warm air advection ahead of them induces ascent and cold air advection behind them induces descent. This configuration could make isentropic descent comparatively more destructive to AEW convection, since it tends to put dry air in the very region where AEWs would otherwise generate precipitation.

Differencing the 0-40% composite and the 80-100% composite yields significantly higher mixing ratios in the northwestern quadrant of the AEW, but slightly lower ones in the southern third (Fig. 9(d)). For the 80-100% composite, the drier air in the northwest quadrant is indicative of isentropic descent and the moister air to the south is consistent with a southward shift in the convection. These differences of 1.5-2.5 g/kg at approximately 870 mb on the 303 K isentropic surface, correspond to differences in equivalent potential temperature of 5-8 K. Some of the moisture differences may result from the increase in precipitation for cases with less isentropic descent (not shown) and thus is only indirectly related to the southward advection of isentropic descent. Nevertheless, large moisture differences outside of regions of significant convection confirm the drying effect of the southward advection of isentropic descent.

The shifts in the location and intensity of convection also appear to affect the velocity field. The 0-40% composite has anomalously weaker northerly flow ahead of it, primarily in the southern quadrant, and anomalously weaker westerly flow south of it. These differences likely result from the tendency for convection to be collocated with low level convergence. As the convection shifts northward from the 80-100% composite to the 0-40% composite, the associated convergence shifts approximately 3° northward. Additionally, due to the stronger central convection, the 0-40% composite has a slightly stronger cyclonic circulation near its center. However, the tendency for isentropic descent to have higher low level static stability

complicates this analysis (Fig. 10). Compared with the 0-40% composite, the 301-305 K lapse rate 200-300 km northwest of the circulation center in the 80-100% composite is up to 9 hPa/K higher. For reference, this layer corresponds to 900 hPa to 830 hPa at the center of the map for a composite of all cases. This inversion, combined with dry air, would be extremely detrimental to convection. Unfortunately, it is difficult to separate these two factors in this analysis.

2) Comparison of Developing and Non-developing AEWs

If isentropic descent does indeed have a significant influence on tropical cyclogenesis, one would expect to see its signature more prominently in the non-developing AEW cases. The composite 303 K mixing ratio and winds and the 500 hPa vertical velocity for developing, non-developing and the difference between the two are shown in Figs. 11 a-c.

The most striking feature in the composite difference is the tendency for the developing cases to have higher mixing ratios northwest of their circulation center and stronger convection near their center(Fig. 11(c)) . The mixing ratio field for the non-developing case demonstrates a clear tendency for the southward advection of drier air to erode the northern edge of the convection. Recall from previous analysis that developing systems tend to have much less isentropic descent within the northeastern quadrant of the circulation (Fig. 9(d)). Although this finding at first seems contradictory with the greater mixing ratios differences in the northwestern quadrant, it may be that the more important factor for tropical cyclogenesis is not whether or not isentropic descent is ingested into the circulation, but how dry it is since it can undergo significant modification before it impacts AEW convection.

It is likely that, when isentropic descent wraps around the back side of the circulation into the northeastern quadrant, it becomes significantly moister due to a longer residence time over warmer water and interaction with precipitation. However, once isentropic descent has reached the back side of the circulation, the front side has already entrained significant amounts of dry air from isentropic descent. Additionally, advection is not the only process affecting the 303 K mixing ratio pattern; the developing AEWs tend to be more convectively active and hence contain more low level moisture resulting from precipitation. Though it is difficult to distinguish the impact of horizontal moisture advection from precipitation in these composites, the northwestward extension of the anomalously dry air from the circulation center suggests that advection of dry air suppresses convection within the northwestern quadrant (Fig. 11(c)). In addition to suppressing the central convection, this advection pattern shifts the region of convection in the non-developing cases southward with respect to the developing cases. In fact, non-developing cases have slightly higher mixing ratios (about 0.5 g/kg) in the southern half of their circulation due to this southward shift in precipitation (Fig. 11(c)).

Developing cases also have a stronger 303 K circulation and enhanced convergence just southeast of the circulation center in association with the enhanced convection. One of the complicating factors in this analysis is the tendency of isentropic descent to be associated with higher static stability (Fig. 11(d)). As suggested by Fig. 4(a), an air column undergoing isentropic descent along the African coast undergoes a large increase in static stability and can advect this southward in the form of a low level inversion. Figure 11(d) shows that non-developing cases have much higher static stability than developing cases, and this difference is roughly collocated with the large differences in mixing ratio between developing and non-

developing cases (Fig. 11(c)). Both low level dry air and high static stability are detrimental to convection and tropical cyclogenesis and it is difficult to separate the two in this analysis. Nevertheless, these results reinforce the notion that isentropic descent is detrimental to tropical cyclogenesis due to its suppression of convection.

4. Synthesis

Our analysis confirms that the SAL forces isentropic descent in the northeastern Atlantic near the northwest African coast. The anomalously high potential temperature of the overlying SAL forces the underlying isentropes downward and thus causes the northerly flow on the eastern flank of the Azores High to descend along the isentropes. One can visualize this descent as northerly flow from the mid-latitudes undercutting the SAL. This strong and persistent descent brings extremely dry air from aloft in the middle latitudes to low levels in the tropical eastern Atlantic. The novelty is that this dry air does not originate from the SAL as many previous studies have suggested.

We have also determined that AEWs exiting the African continent ingest a significant fraction of this airmass into their circulation and that it is detrimental to their convection and future tropical cyclogenesis, since it places extremely dry at low levels and is often associated with high static stability. One can view the interaction between AEWs and isentropic descent as a multistage process. AEWs entering the eastern Atlantic tend to have a low level cyclonic circulation near 850 hPa. Upon leaving the African continent, the northerly flow ahead of their circulation joins with the persistent northerly flow along the northwest African coast north of 20°N. This process brings dry air from the mid-latitudes into the AEW circulation

and may suppress the convection within the AEW. The concentration of this dry air on the front side of the AEW low level circulation, the same region where the AEW structure forces adiabatic ascent, may have a disproportionate effect of its convection.

However, the dry air from isentropic descent undergoes significant modification as it comes into contact with surface moisture fluxes from the ocean. In fact, warmer water north of 15°N along the African coast may diminish the negative impacts of isentropic descent by moistening and destabilizing it before it can reach AEWs to the south. Thus, isentropic descent is less effective at inhibiting tropical cyclogenesis during September and anomalously warm water north of about 15°N may even favor an increase in downstream convection and tropical cyclones in the eastern Atlantic.

While not the primary determinant of tropical cyclogenesis, the results presented here suggest that isentropic descent should be considered as one of the ingredients impacting cyclogenesis acting independently of other factors such as vertical wind shear. The results also support the view of Braun (2010) in that there are other sources of dry air in the eastern Atlantic beyond the SAL. In this case, the SAL plays an active role in localizing and enhancing the isentropic descent over eastern Atlantic.

Acknowledgments.

This work is supported in part by NSF grant ATM-0847323 and NOAA grant NA06OAR4810187.

The data for this study are from the Research Data Archive (RDA) which is maintained by the Computational and Information Systems Laboratory (CISL) at the National Center for Atmospheric Research (NCAR). NCAR is sponsored by the National Science Foundation

(NSF). The original data are available from the RDA (http://dss.ucar.edu) in dataset number ds083.2.

REFERENCES

Berry, G. J., C. D. Thorncroft, and T. Hewson, 2007: African easterly waves during 2004 analysis using objective techniques. *Monthly Weather Review*, **135**, 1251–1267.

Braun, S. A., 2010: Re-evaluating the role of the saharan air layer in atlantic tropical cyclogenesis and evolution. *Monthly Weather Review*, **138**, 2007–2037.

Carlson, T. N., 1969: Some remarks on african disturbances and their progress over the tropical atlantic. *Monthly Weather Review*, **97 (10)**, 716–726.

Carlson, T. N. and J. M. Prospero, 1969: Synoptic histories of three african disturbances that developed into atlantic hurricanes. *Monthly Weather Review*, **97 (3)**, 256–276.

Carlson, T. N. and J. M. Prospero, 1972: The large-scale movement of saharan air outbreaks over the northern equatorial atlantic. *Journal of Applied Meteorology*, **11**, 283–297.

DeMaria, M., J. A. Knaff, and B. H. Connell, 2001: A tropical cyclone genesis parameter for the tropical atlantic. *Weather and Forecasting*, **16 (10)**, 219–233.

Dunion, J. P. and C. S. Velden, 2004: The impact of the saharan air layer on atlantic tropical cylcone activity. *Bulletin of the American Meteorological Society*, **85**, 353–365.

Gray, W. M., 1968: Global view of the origin of tropical disturbances and storms. *Monthly Weather Review*, **96 (10)**, 669–700.

Karyampudi, V. M. and T. N. Carlson, 1988: Analysis and numerical simulations of the saharan air layer and its effect on easterly wave disturbances. *Journal of the Atmospheric Sciences*, **45 (21)**, 3102–3136.

Karyampudi, V. M. and H. F. Pierce, 2002: Synoptic-scale influence of the saharan air layer on tropical cyclogenesis over the eastern atlantic. *Monthly Weather Review*, **130**, 3100–3128.

Kiladis, G. N., C. D. Thorncroft, and N. M. J. Hall, 2006: Three-dimensional structure and dynamics fo african easterly waves. part i: Observations. *Journal of the Atmospheric Sciences*, **63**, 2212–2230.

Pasch, R. J., L. A. Avila, and J.-G. Jiing, 1998: Atlantic tropical systems of 1994 and 1995: A comparison of a quiet season to a near-record-breaking one. *Monthly Weather Review*, **126**, 1106–1123.

Rodwell, M. J. and B. J. Hoskins, 1996: Monsoons and the dynamics of deserts. *Quarterly Journal of the Royal Meterological Society*, **122**, 1385–1404.

Rodwell, M. J. and B. J. Hoskins, 2001: Subtropical anticyclones and summer monsoons. *Journal of Climate*, **14**, 3192–3211.

Thorncroft, C. and K. Hodges, 2001: African easterly wave variability and its relationship to atlantic tropical cyclone activity. *Journal of Climate*, **14**, 1166–1179.

List of Tables

TABLE 1. Summary statistics for selected cases showing average latitude of circulation and average and median fractions of isentropic descent within 300 km of center.

	All	July	Aug.	Sept.
All Cases				
Avg. Lat.	11.79	12.21	12.54	10.57
Avg. %	69.24	78.87	74.61	54.41
Med. %	76.2	93.25	80.4	50.5
Total Cases	191	58	70	63
Developing				
Avg. Lat.	11.58	11	11.78	11.55
Avg. %	57.02	58.74	58.04	55.8
Med. %	50.5	70.1	55.65	49.95
Total Cases	45	5	18	22
Non-Developing				
Avg. Lat.	11.86	12.32	12.81	10.05
Avg. %	73.01	80.76	80.35	53.66
Med. %	84.45	94.8	90.7	50.5
Total Cases	146	53	52	41

TABLE 2. Comparison between developing and non-developing systems in relation to fraction of airmass from isentropic descent.

	All	July	Aug.	Sept.
Developing				
0-40%	14	2	5	7
40-80%	16	1	6	9
80-100%	15	2	7	6
Non-Developing				
0-40%	24	5	4	15
40-80%	45	16	14	15
80-100%	77	32	34	11
Ratio				
0-40%	0.37	0.29	0.56	0.32
40-80%	0.26	0.06	0.3	0.38
80-100%	0.16	0.06	0.17	0.35

List of Figures

9 Composite 303 K mixing ratio (g/kg), 500 mb vertical velocity (mb/day), and 303 K winds for cases with 0-40% of their airmass with a history of isentropic descent (a), 40-80% (b), 80-100% (c), and the difference between the 0-40% composite and 80-100% composite 40

10 Difference in 301-305 K lapse rate between cases with 0-40% of airmass with a history of isentropic descent and 80-100% for all cases 41

11 Composite 303 K mixing ratio (g/kg), 500 mb vertical velocity (mb/day), and 303 K winds for developing cases (a), non-developing cases (b), the difference between the two (c), and the difference in 301-305 K lapse rate (mb/K) between developing and non-developing cases 42

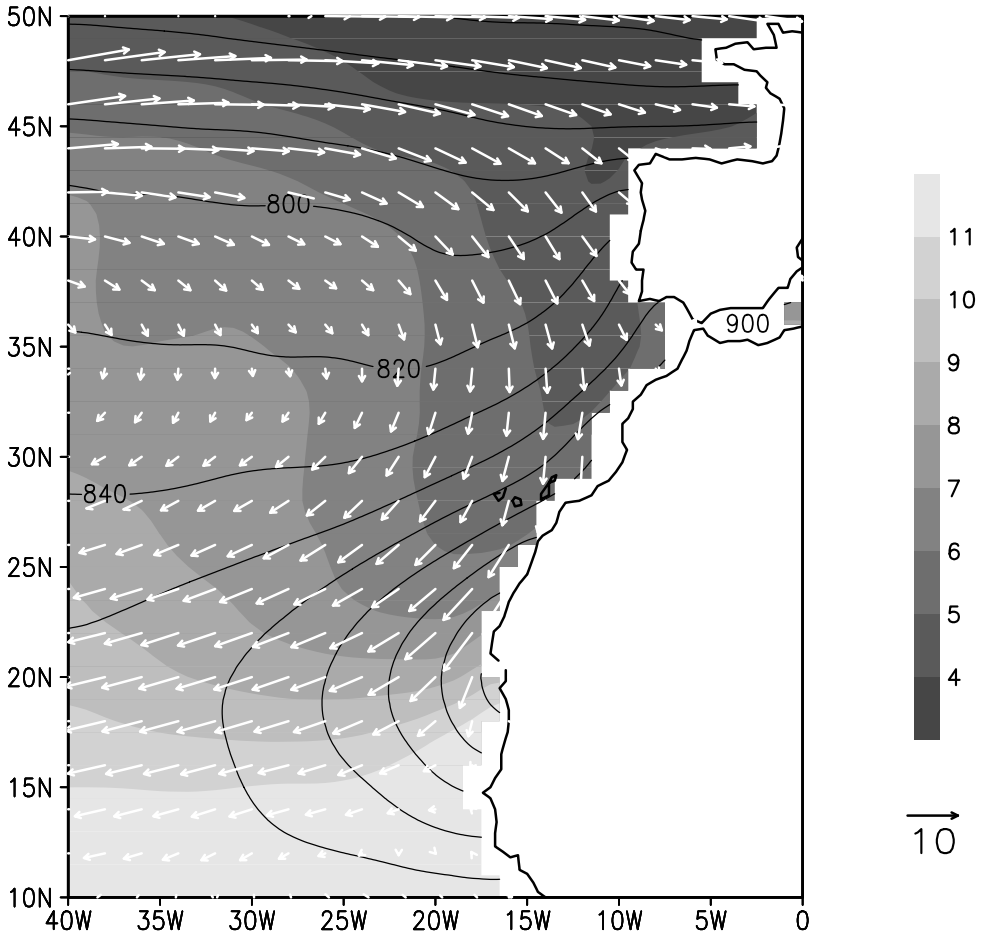

FIG. 1. Average pressure (mb), mixing ratio (g/kg), and winds for JAS on the 303 K isentropic surface, using GFS analyses from 2000 to 2008

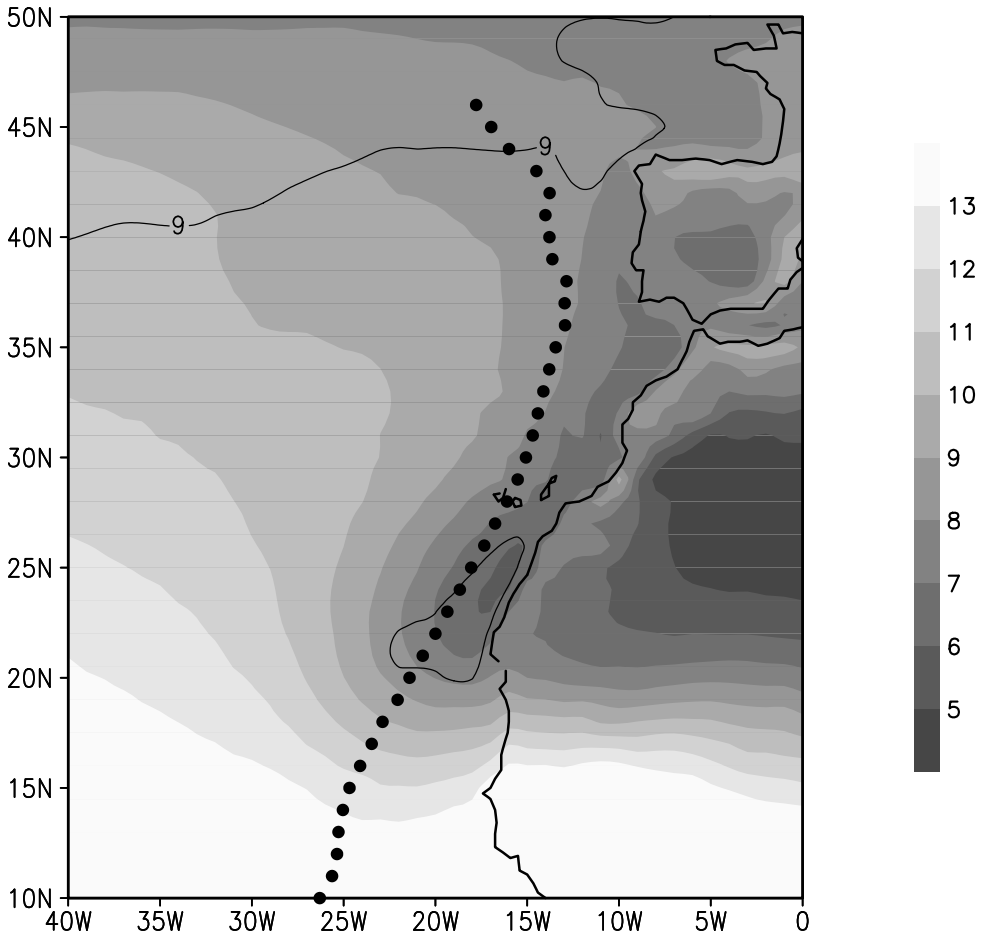

FIG. 2. Composite 301 K trajectory, shaded average 925 mb mixing ratio (g/kg), and contoured average 1000 mb wind (m/s) for JAS. Only the 9 m/s wind speed contour is shown.

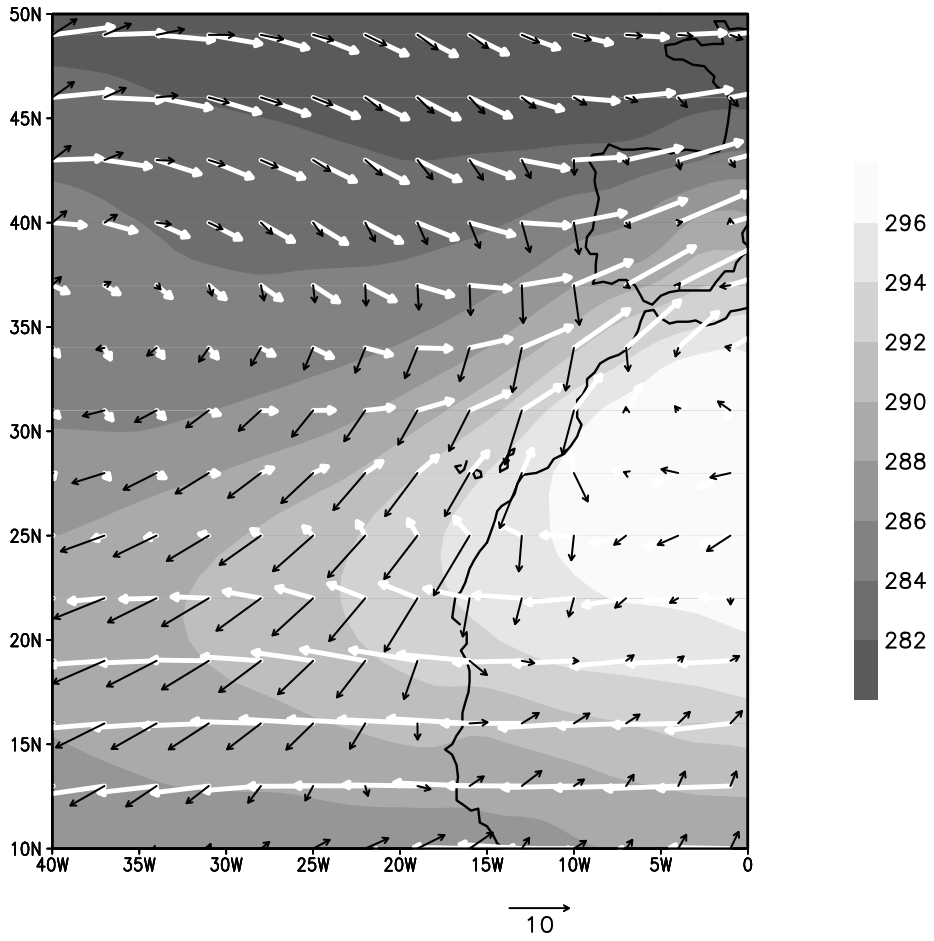

FIG. 3. Average wind vectors at 600 mb (bold, white) and 975 mb (narrow, black) and average 800 mb temperature (K) for JAS

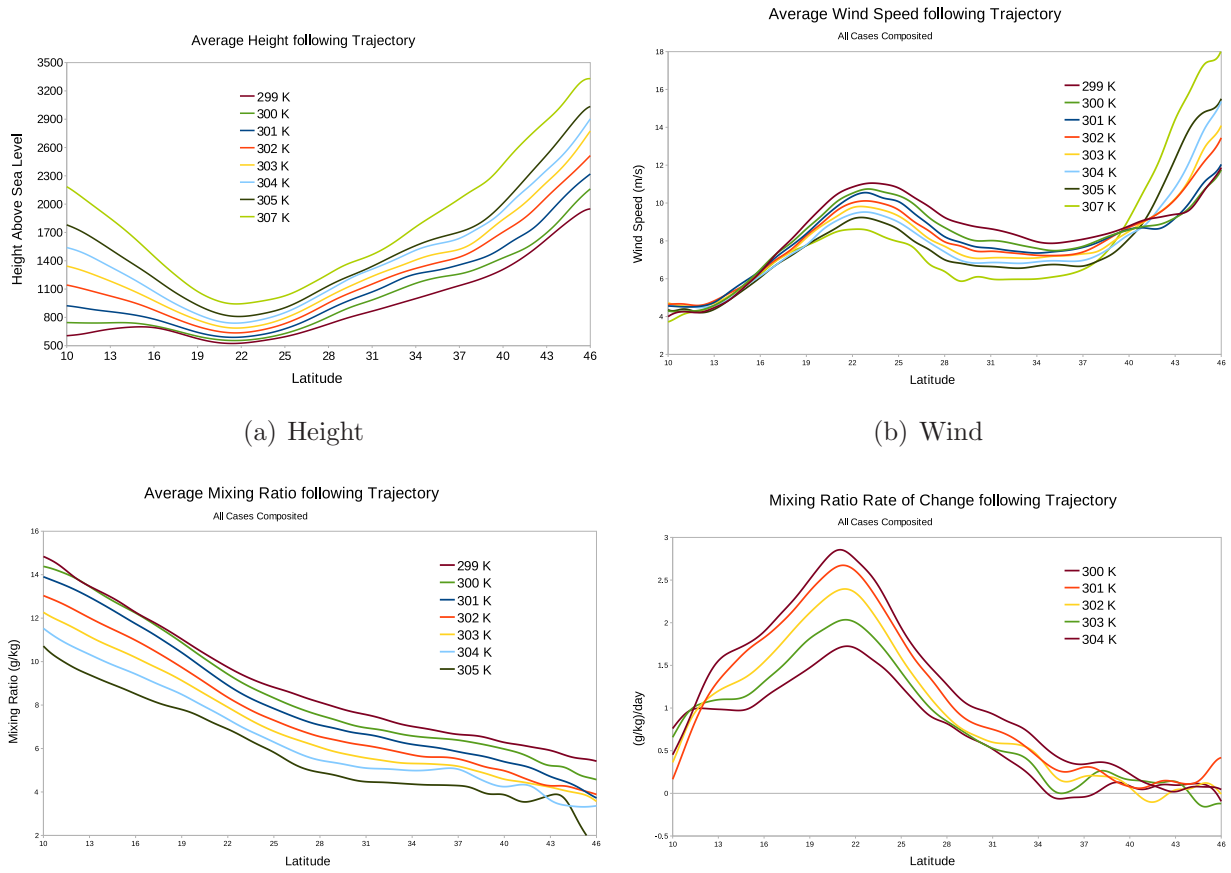

(a) Height

(b) Wind

(c) Mixing Ratio

(d) Mixing Ratio Chage

FIG. 4. Quantities averaged along the composite trajectory, including (a) height (m), (b) wind (m/s), (c) mixing ratio (g/kg), and (d) time rate of change of mixing ratio (g/kg/day)

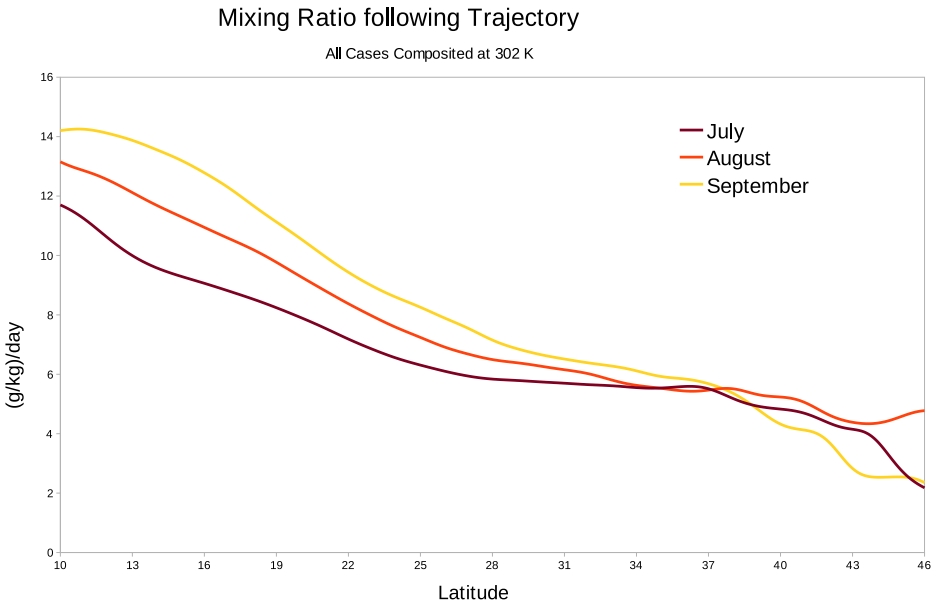

FIG. 5. Mixing ratio (g/kg) averaged along composite trajectory by month

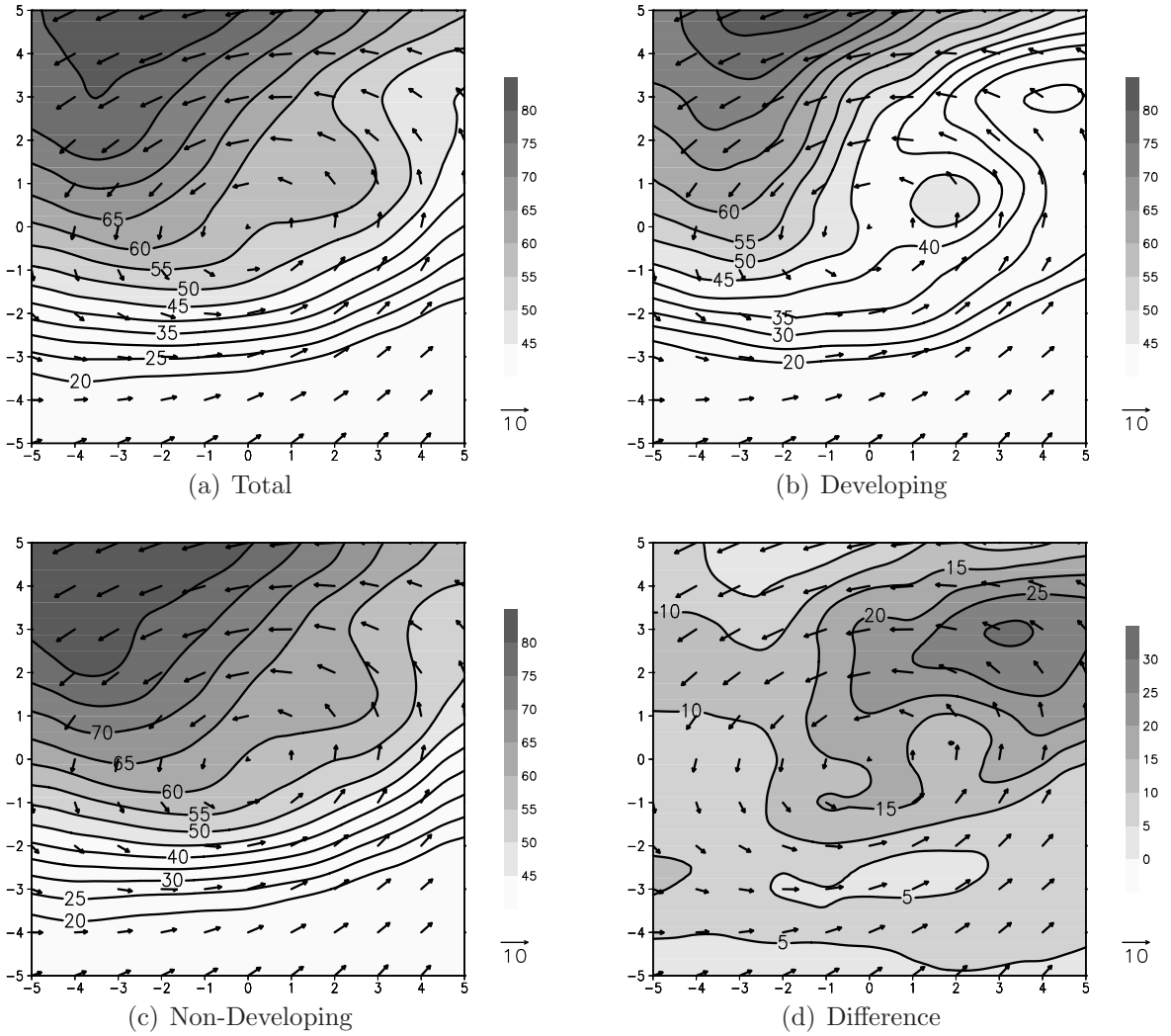

FIG. 6. Fequency at which different regions of the circulation contain airmass with a history of isentropic descent (values in percent of cases)

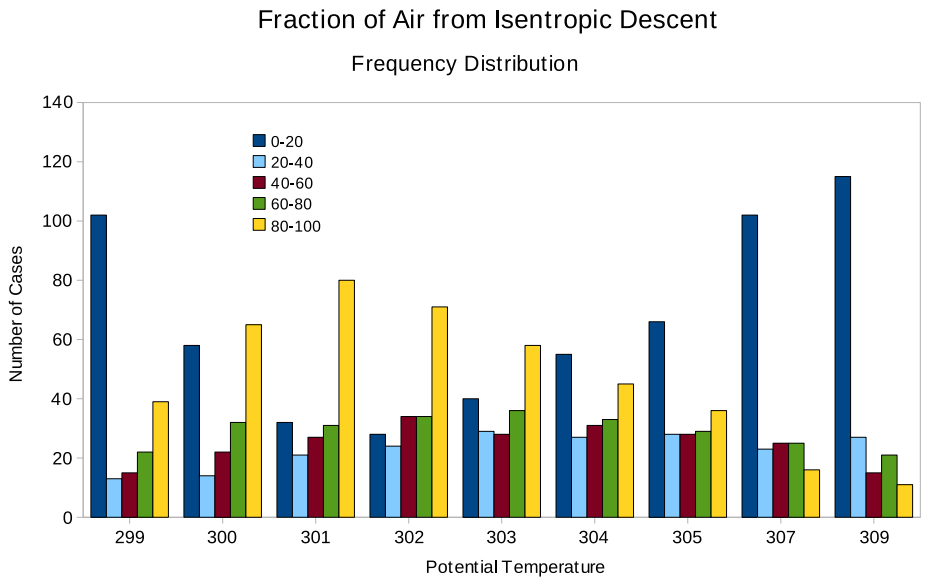

FIG. 7. Fraction of circulation with a history of isentropic descent grouped by potential temperature. For a given potential temperature, each bar represents the fraction of circulation (0-20%,20-40%,etc.) containing this air mass. The y-axis shows the number of cases in each category.

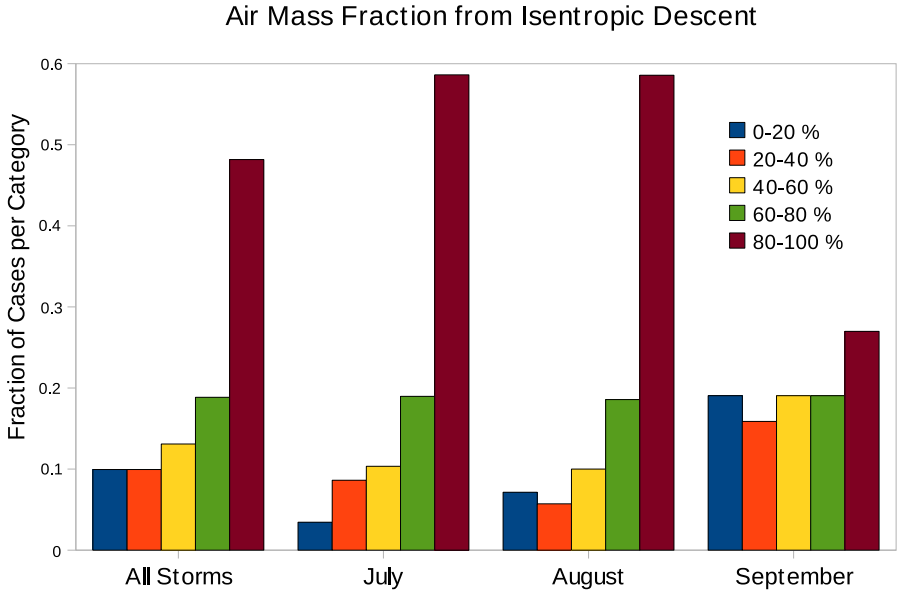

FIG. 8. All cases grouped by the fraction of circulation containing air with a history of isentropic descent. The y-axis shows the fraction of cases in each category

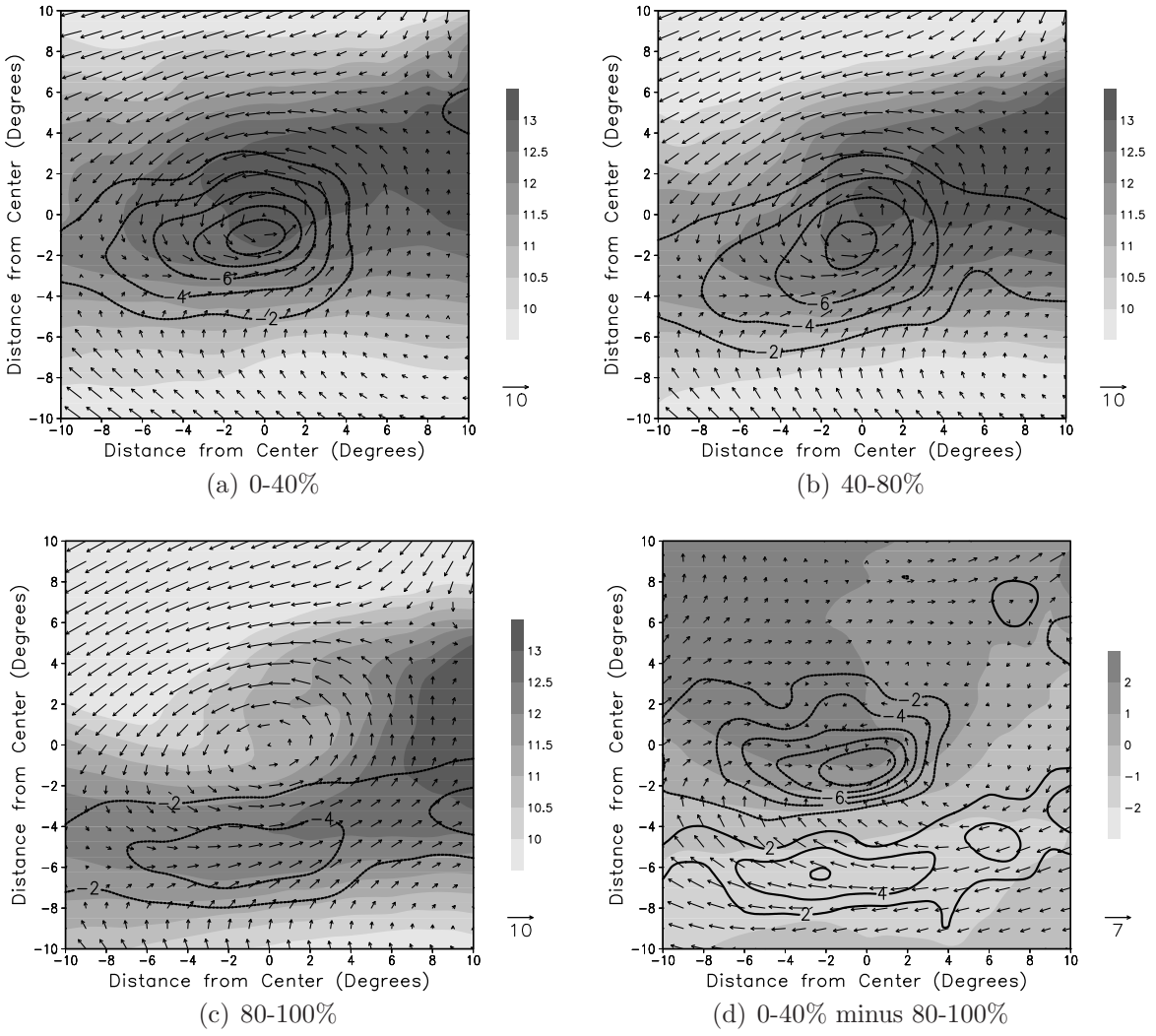

FIG. 9. Composite 303 K mixing ratio (g/kg), 500 mb vertical velocity (mb/day), and 303 K winds for cases with 0-40% of their airmass with a history of isentropic descent (a), 40-80% (b), 80-100% (c), and the difference between the 0-40% composite and 80-100% composite

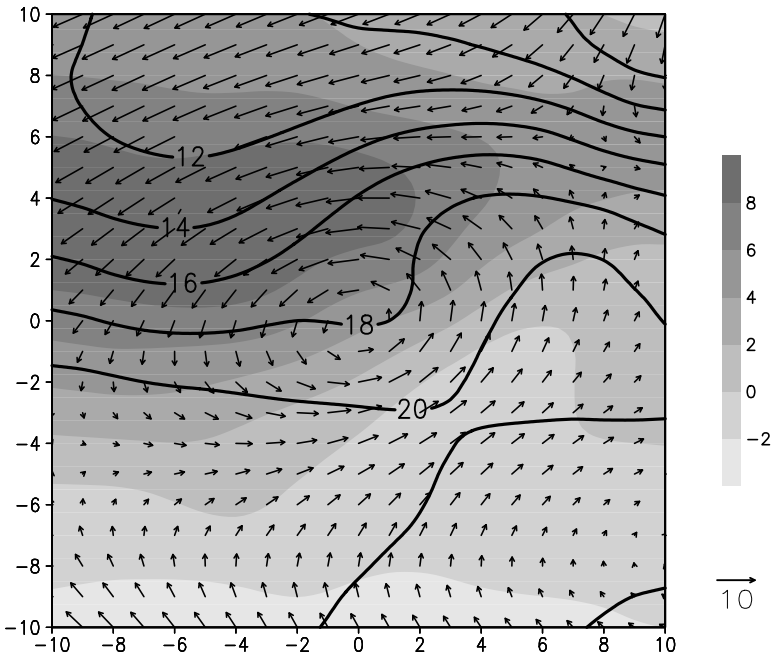

FIG. 10. Difference in 301-305 K lapse rate between cases with 0-40% of airmass with a history of isentropic descent and 80-100% for all cases

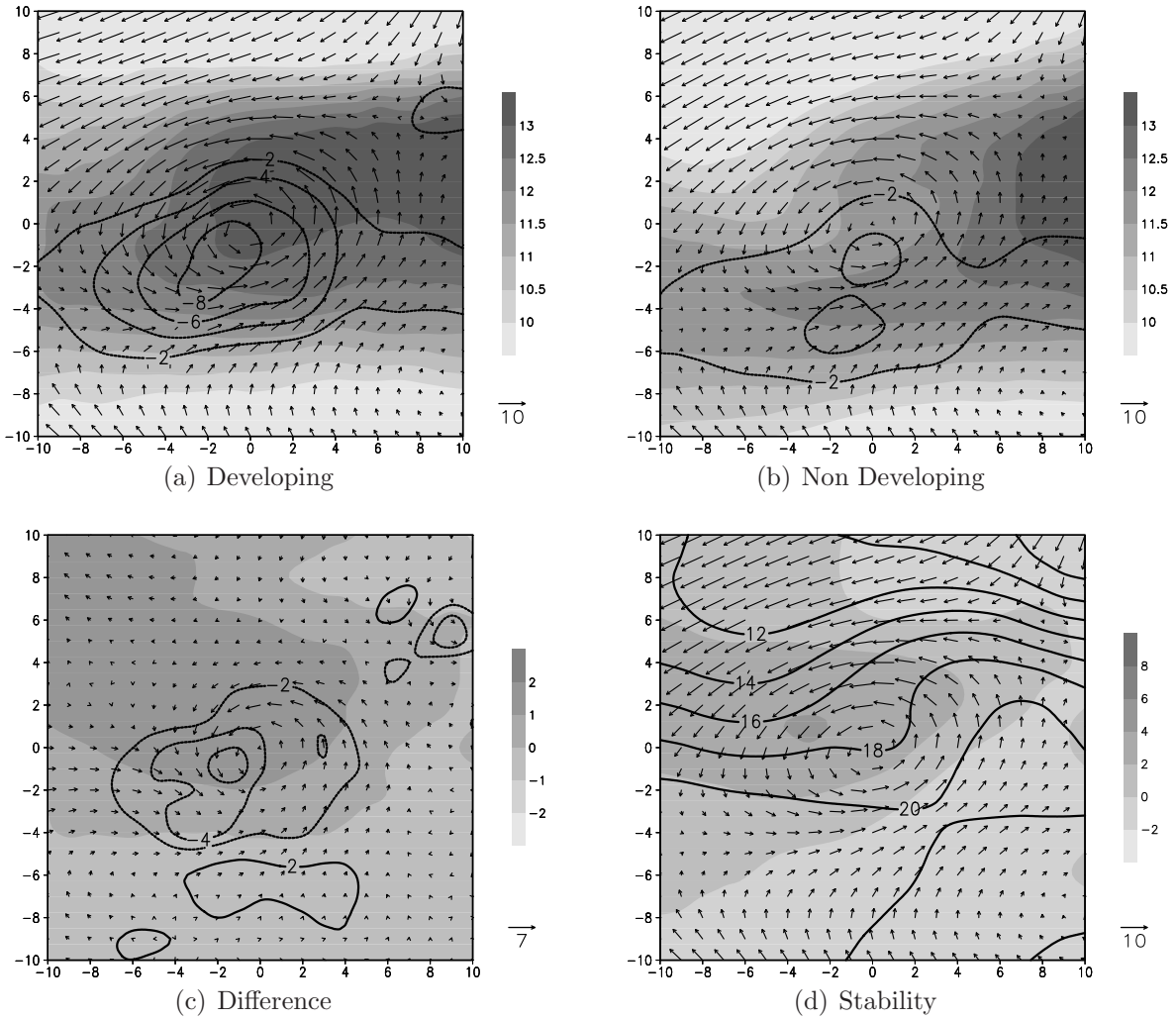

FIG. 11. Composite 303 K mixing ratio (g/kg), 500 mb vertical velocity (mb/day), and 303 K winds for developing cases (a), non-developing cases (b), the difference between the two (c), and the difference in 301-305 K lapse rate (mb/K) between developing and non-developing cases